Journal of ELECTRONIC MATERIALS, Vol. 44, No. 12, 2015
DOI: 10.1007/s11664-015-4038-4

Effect of Titanium Content on Dielectric and Energy Storage Properties of (Pb,La,Sr)(Zr,Sn,Ti)O_3 Ceramics

XIAOZHEN SONG,[1] YONG ZHANG,[1,2] YONGZHOU CHEN,[1] QIAN ZHANG,[1] JIA ZHU,[1] and DONGLIANG YANG[1]

1.—Beijing Key Laboratory of Fine Ceramics, State Key Laboratory of New Ceramics and Fine Processing, Institute of Nuclear and New Energy Technology, Tsinghua University, Beijing 100084, People's Republic of China. 2.—e-mail: yzhang@tsinghua.edu.cn

The dielectric and energy storage properties of lead lanthanum strontium zirconate stannate titanate [$(Pb_{0.92}La_{0.04}Sr_{0.02})((Zr_{0.70}Sn_{0.30})_{1-x}Ti_x)O_3$] ceramics were investigated as a function of x ($0.07 \le x \le 0.13$). With increasing titanium content, the tolerance factor increased, resulting in decreased stability of antiferroelectric phase in the ceramics. As the titanium content was increased, the maximum dielectric constant increased and the temperature of the dielectric maximum shifted to lower values. According to the polarization–electric field hysteresis loops, both the charged and discharged energy densities increased consistently with the increase of titanium content. The unreleased energy densities also showed a systematic trend. From charge–discharge measurements based on the resistance load circuit, the released energy densities and power densities as a function of discharge time were determined over the investigated composition range.

Key words: PLSZST ceramics, titanium content, dielectric properties, energy storage

INTRODUCTION

Lead lanthanum zirconate stannate titanate [(Pb,La)(Zr,Sn,Ti)O_3, PLZST] antiferroelectric (AFE) ceramic materials have been studied extensively over the past several decades for applications in high-energy-storage capacitors[1,2] and high-strain actuators.[3,4] The greatest improvement has been achieved by doping various amounts of A- or B-site (ABO_3) additives.

It was reported that strontium addition can suppress hysteresis of PLZST ceramics, but this has limited merit because it causes an increase in the antiferroelectric–ferroelectric (AFE–FE) switching field.[5] In addition, previous studies mainly focused on the effect of B-site variations on the electrical properties of the PLZST ceramics; for example, variations in the Ti:Sn and Zr:Sn ratios were evaluated in the PLZST ceramics. It was found that the increase of Zr^{4+} content could decrease the dielectric constant and the switching field of the PLZST ceramics,[6] while the switching field increased with increase of the Sn^{4+} content in PLZST ceramics.[7] The influence of varying the titanium content on the microstructure and dielectric properties is needed for further investigation of the PLZST ceramics. There have been many earlier attempts to investigate the energy storage properties of antiferroelectric ceramics. In general, such energy storage density measurements were limited to employment of polarization–electric field (P–E) hysteresis loops, whereas there are few reports on measurements of charge–discharge curves.

In the present study, the dielectric and energy storage performance of $(Pb_{0.92}La_{0.04}Sr_{0.02})((Zr_{0.70}Sn_{0.30})_{1-x}Ti_x)O_3$ (PLSZST) ceramics was investigated as a function of x ($0.07 \le x \le 0.13$). The PLSZST ceramics were synthesized by the conventional solid-state reaction method. The microstructure and dielectric properties of the studied ceramics were analyzed to explain their energy storage performance. The energy storage density of these PLSZST ceramics was studied by both P–E hysteresis loop and discharge curve measurements.

(Received June 22, 2015; accepted September 3, 2015; published online September 21, 2015)

The objective of this work is to study the influence of the titanium content on the dielectric and energy storage properties of these PLSZST ceramics.

EXPERIMENTAL PROCEDURES

$(Pb_{0.92}La_{0.04}Sr_{0.02})((Zr_{0.70}Sn_{0.30})_{1-x}Ti_x)O_3$ (PLSZST) powders with different titanium contents (x = 7 mol%, 8 mol%, 9 mol%, 10 mol%, 11 mol%, 13 mol%) were prepared by the traditional solid-state reaction method. High-purity raw materials of lanthanum nitrate [$La(NO_3)_3{\cdot}6H_2O$, 98.0% purity], strontium carbonate ($SrCO_3$, 99.0% purity), zirconia (ZrO_2, 99.0% purity), lead tetroxide (Pb_3O_4, 95.0% purity) (Sinopharm Chemical Reagent Co., Ltd., Beijing, China), tin dioxide (SnO_2, 99.5% purity) (Tianjin Guangfu Fine Chemical Institute Co., Ltd., Tainjin, China), and titanium dioxide (TiO_2, 99.0% purity) (Tainjin Fuchen Chemical Reagent Factory, Tainjin, China) were used. These compounds were weighed in stoichiometric ratios and mixed by ball-milling. After drying, the mixture was calcined at 1070°C for 2 h to prepare PLSZST powder.

To improve the sintering and dielectric properties of the PLZST ceramics, $Pb(Mg_{0.5}W_{0.5})O_3$ (PMW) and MnO_2 were added to the PLSZST powders. Such addition of $Pb(Mg_{0.5}W_{0.5})O_3$ and MnO_2 aimed to decrease the sintering temperature and dielectric loss, respectively. $Pb(Mg_{0.5}W_{0.5})O_3$ was synthesized by a two-stage process starting from the raw materials Pb_3O_4, WO_3, and $(MgCO_3)_4{\cdot}Mg(OH)_2{\cdot}5H_2O$ (Sinopharm Chemical Reagent Co. Ltd., Beijing, China). The wolframite precursor $MgWO_4$ was prepared by calcining a stoichiometric mixture of $(MgCO_3)_4{\cdot}Mg(OH)_2{\cdot}5H_2O$ and WO_3 at 1000°C for 2 h. Then, a stoichiometric amount of Pb_3O_4 was mixed with $MgWO_4$, and the mixture was calcined at 800°C for 2 h to obtain PMW powder. Then, the PLSZST powders were mixed with 5 wt.% PMW and 0.05 wt.% MnO_2 by ball-milling for 4 h, and the resultant slurry was dried and finally sifted through 120 meshes. The final powders were granulated by adding poly(vinyl alcohol) (PVA, 5 wt.%) as binder. The powders were uniaxially pressed to form pellets under a pressure of 4 MPa. All samples were sintered in air at 1140°C for 2 h. To avoid PbO loss, a PbO-rich atmosphere was maintained by placing powders of the same composition during the sintering process. After sintering, silver paste was printed onto both sides of the disks and subsequently fired at 600°C for 20 min.

An x-ray diffractometer (XRD, D8 Advance; Bruker AXS, Karlsruhe, Germany) was used to investigate the phase evolution of the synthesized PLSZST powders. The surface morphology of the samples was observed by scanning electron microscopy (SEM, FEI Model Quanta 200 FEG). The capacitance and loss tangent were measured using an inductance–capacitance–resistance (*LCR*) meter (model 4284A; Hewlett-Packard, Palo Alto, CA) at frequency of 1 kHz over the temperature range from −55°C to 150°C with a heating rate of 5°C/ min. Polarization–electric field (*P–E*) hysteresis loops were measured using a modified Sawyer-Tower circuit. During testing, the samples were submerged in silicone oil to prevent arcing. A charge–discharge measurement system based on a resistance load circuit, reported elsewhere,[8] was employed to measure the discharge curves of the samples after charging at 6 kV/mm. The load resistance applied this measurement was 3 MΩ.

RESULTS AND DISCUSSION

XRD results of the as-calcined PLSZST powders with various titanium contents are illustrated in Fig. 1a. It can be seen that all the samples exhibited pure perovskite structure. The intensities of the reflections decreased slightly with the increase of titanium content from 7 mol% to 10 mol%, then increased slowly with increasing titanium content from 11 mol% to 13 mol%. As shown in Fig. 1b, in the enlarged region located at ~44°, a shoulder in the (200) reflection peak appears for all the samples, indicating coexistence of rhombohedral and tetragonal phases. These Bragg reflections from the (200) peak demonstrate that these PLSZST compositions are in proximity to the morphotropic phase boundary (MPB). As the titanium content was increased, this broad peak did not split into two peaks. However, the results indicated that titanium substitution stabilized the tetragonal phase over the rhombohedral phase, as previously indicated in the PLZST phase diagram.[5]

The phase stability of the perovskite structure can also be evaluated in terms of the tolerance factor t, which is defined as follows:

$$t = \frac{R_A + R_O}{\sqrt{2}(R_B + R_O)}, \quad (1)$$

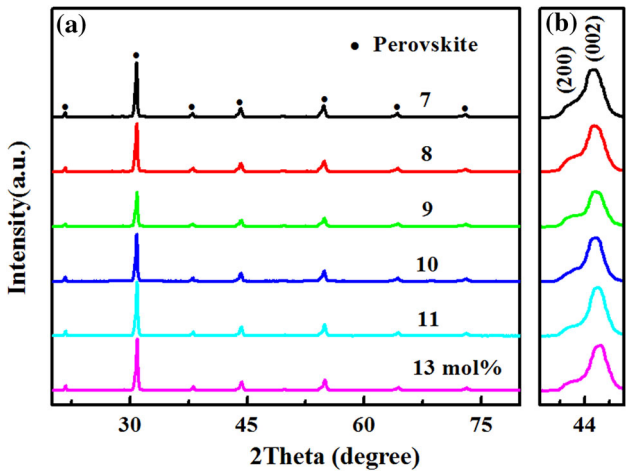

Fig. 1. (a) X-ray diffraction patterns for PLSZST powders with different titanium contents; (b) enlarged region located at ~44°.

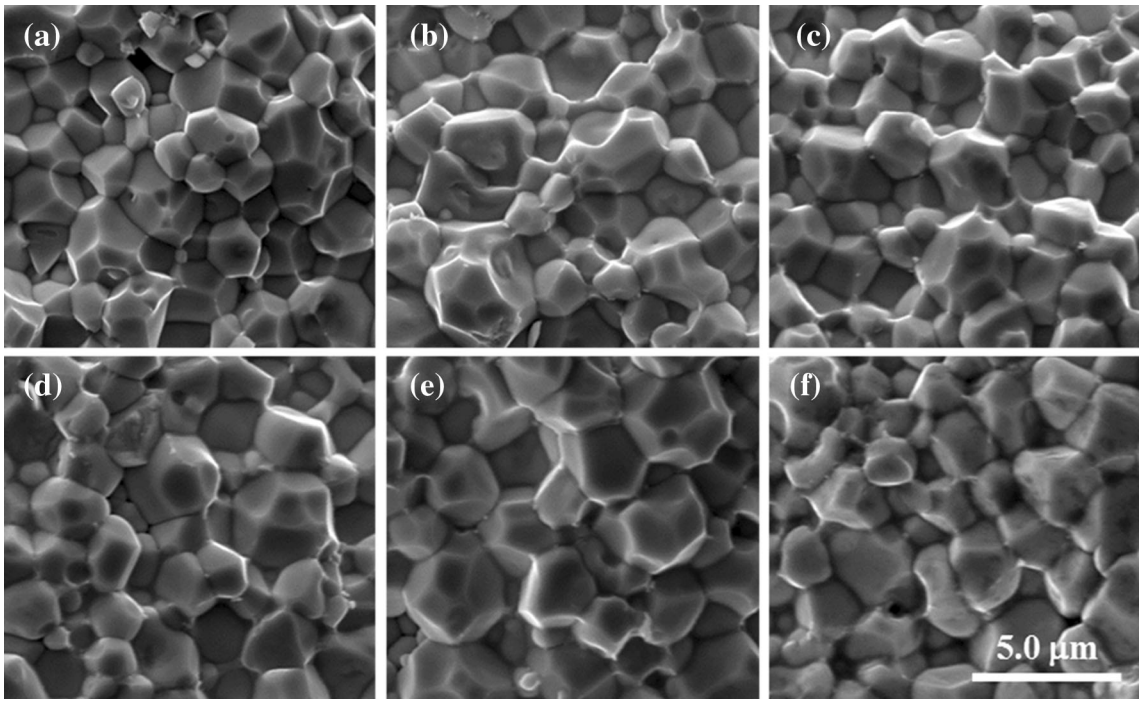

Fig. 2. SEM micrographs of the PLSZST ceramics sintered at 1140°C for 2 h with different titanium contents: (a) 7 mol%, (b) 8 mol%, (c) 9 mol%, (d) 10 mol%, (e) 11 mol%, (f) 13 mol%.

where R_A, R_B, and R_O are the ionic radii of the A-site cation, B-site cation, and oxygen anion, respectively.

$$R_A = 0.92r_{Pb^{2+}} + 0.04r_{La^{3+}} + 0.02r_{Sr^{2+}}, \quad (2)$$

$$R_B = 0.70(1-x)r_{Zr^{4+}} + 0.30(1-x)r_{Sn^{4+}} + xr_{Ti^{4+}}, \quad (3)$$

where $0.70(1-x)$, $0.30(1-x)$, and x are the relative contents of Zr^{4+}, Sn^{4+}, and Ti^{4+}, respectively. When $t > 1$, the FE phase is stabilized; when $t < 1$, the AFE phase is stabilized.[9] The ionic radii of Pb^{2+}, La^{3+}, Sr^{2+}, Zr^{4+}, Sn^{4+}, Ti^{4+}, and O^{2-} are 1.49 Å, 1.36 Å, 1.44 Å, 0.72 Å, 0.69 Å, 0.60 Å, and 1.35 Å, respectively.[10] According to these formulae, the calculated tolerance factor t values were 0.9655, 0.9660, 0.9665, 0.9670, 0.9675, and 0.9685 for the samples with titanium content of 7 mol%, 8 mol%, 9 mol%, 10 mol%, 11 mol%, and 13 mol%, respectively. When the value of t is close to 1, the perovskite phase will be formed.[11] The value of t increased from 0.9655 to 0.9685 in the titanium content range of 7 mol% to 13 mol%. It is clearly shown that the samples with larger t values were more easily induced from the antiferroelectric (AFE) to ferroelectric (FE) state, which is in agreement with the XRD patterns of the samples. Therefore, the AFE behaviors of the PLSZST ceramics with higher titanium contents were not stable under an external electric field.[12]

SEM micrographs of the fracture surfaces of the PLSZST ceramics with different titanium contents are shown in Fig. 2. These micrographs indicate that no abnormal grain growth was observed, resulting in homogeneous fine-grained microstructure. As shown in Fig. 2, the average grain size is in the range of 1 μm to 4 μm. Furthermore, a slight increase in grain size was observed with increasing titanium content, which may be attributed to the good sinterability of titanium.

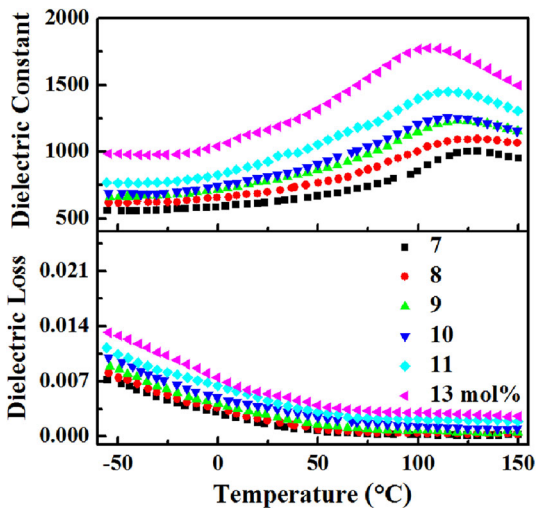

Fig. 3. Temperature dependence of dielectric constant and dielectric loss of the PLSZST ceramics with different titanium contents. The measurement frequency for each sample was 1 kHz.

The effect of the titanium content on the dielectric–temperature characteristic curves of the PLSZST ceramics over the temperature range of

Table I. Maximum dielectric constant (ε_m) and corresponding temperature (T_{max}) for the PLSZST ceramics at 1 kHz

Ti content (mol%)	7	8	9	10	11	13
ε_m	1003	1094	1233	1258	1452	1779
T_{max} (°C)	129.7	129.7	119.6	114.6	114.9	104.8

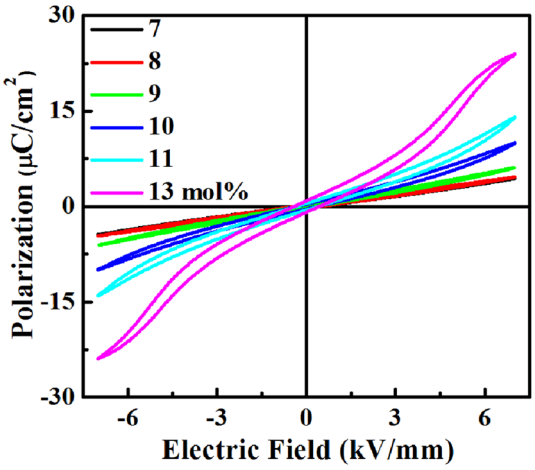

Fig. 4. *P–E* hysteresis loops for the PLSZST ceramics with different titanium contents.

−50°C to 150°C is illustrated in Fig. 3. It can be seen that, with the increase of titanium content, both the dielectric constant and dielectric loss of the PLSZST ceramics increased. Moreover, Table I presents the variation of the maximum dielectric constant (ε_m) and corresponding temperature (T_{max}) as a function of titanium content. As illustrated in Table I, the temperature of the dielectric constant maximum, T_{max}, shifts to lower values with increasing titanium content. Thus, increase in the titanium content results in an increase in the dielectric constant and a reduction in T_{max}.

It can be seen that the dielectric constant of the PLSZST ceramics reaches a maximum value over the entire measurement temperature range. The dielectric constant of the PLSZST ceramics is determined by the relative displacement of the B-site ions: the larger the relative displacement between the O^{2-} ions and B-site ions, the higher the dielectric constant. The radius of Ti^{4+} ion is smaller than that of Zr^{4+} and Sn^{4+} ions, thereby increasing the tolerance factor upon substitution and increasing the space in which the B-site cation is allowed to vibrate, which leads to the higher dielectric constant of the PLSZST ceramics with higher titanium contents. T_{max} shifts to lower temperature with increasing titanium content, which can be explained

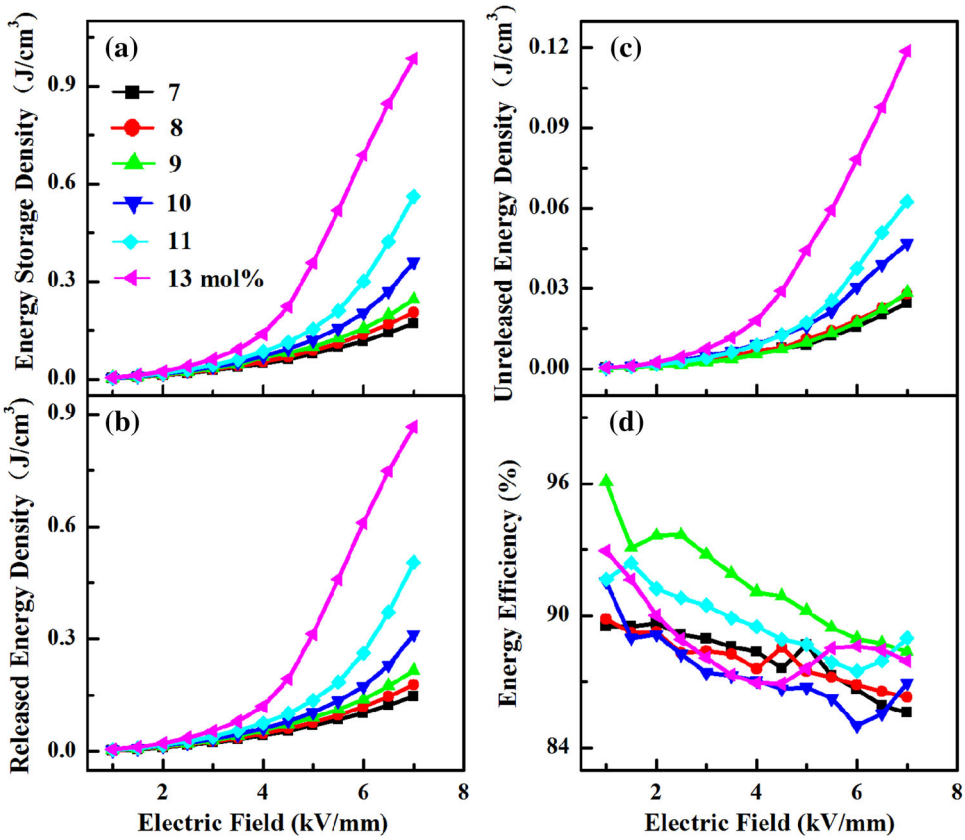

Fig. 5. The charged (a), discharged (b), and unreleased (c) energy densities and energy efficiency (d) as a function of electric field for the PLSZST ceramics with different titanium contents.

by the optical soft mode frequency ω_A^2 of the AFE mode,[3] which can be expressed by Eq. 4:

$$\omega_A^2 = (1/\mu)[(\mathrm{LRF}) - (\mathrm{SRF}) + \gamma T] = K(T - T_{\max}), \tag{4}$$

where μ is the reduced mass, LRF is the long-range Coulombic force, SRF is the short-range force, γT is the perturbation of the harmonic approximation from the inharmonic contribution, and K is a positive constant. The larger distortion of the crystal lattice caused by the substitution of Ti^{4+} with smaller radius for B-site Zr^{4+} and Sn^{4+} increases the vibrational frequency of the AFE mode. As can be seen from Eq. 4, $T_{\max}$ should shift to a lower temperature with the increase of titanium content.

Figure 4 shows the *P–E* hysteresis loops of these PLSZST ceramics as a function of titanium content. With increasing titanium content, one observes a transition from an almost linear hysteresis loop for titanium content of 7 mol% to a double hysteresis loop for titanium content of 13 mol%, representing a typical antiferroelectric. In addition, the maximum polarization of these ceramics increased significantly with increasing titanium content. The AFE–FE switching field decreased as the titanium content was increased. This result reveals that the stability of the antiferroelectric phase decreases with increasing titanium content, in agreement with the XRD results and dielectric properties.

The energy storage density J of the PLSZST ceramics was calculated from the *P–E* hysteresis loops according to Eq. 5[13]:

$$J = \int_0^{E_{\max}} D\mathrm{d}E, \tag{5}$$

where E is the external applied field and D is the electrical displacement.

For dielectrics with high permittivity, Eq. 5 can be written as[13]

$$J = \int_0^{E_{\max}} P\mathrm{d}E. \tag{6}$$

Based on Eq. 6, the J value of the PLSZST ceramics can be obtained by numerical integration of the area between the polarization and the curves of the *P–E* loops. The charged energy density (J_c) of the PLSZST samples is equal to the integral of the area enclosed by the charge curve and the *y*-axis. The discharged energy density (J_d) is equal to the integral of the area enclosed by the discharge curve and the *y*-axis. The unreleased energy density or the energy loss is equal to the integral of the area enclosed by the charge and discharge curves and the *y*-axis. In addition, the energy efficiency (η) can be defined as

$$\eta = \frac{J_d}{J_c} \times 100\%. \tag{7}$$

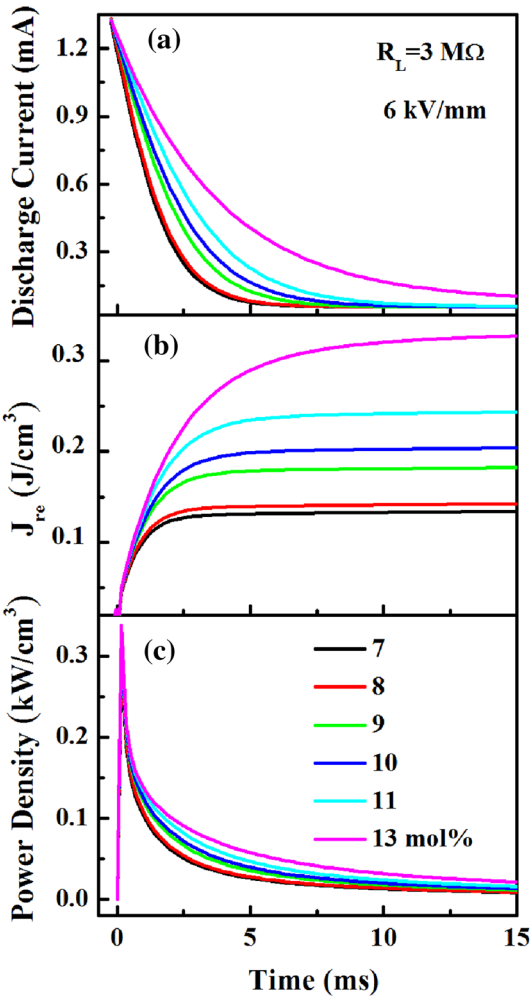

Fig. 6. Discharge curves (a), released energy densities (J_{re}) (b), and power densities (c) for the PLSZST ceramics with different titanium contents after charging at 6 kV/mm.

The energy storage properties of the PLSZST ceramics with various titanium contents are illustrated in Fig. 5. It can be seen that the values of J_c, J_d, and unreleased energy density of the PLSZST ceramics increased with increase of the applied electric field. Moreover, with increasing titanium content, the values of both J_c and J_d increased. The values of η for the samples are in the range from 85% to 96%. In particular, when the titanium content reached 9 mol%, the ceramic showed a maximum efficiency.

The discharged energy density calculated from the hysteresis loop cannot represent the real energy density released from the sample. Therefore, a specially designed charge–discharge experiment was performed to validate the released energy density in these PLSZST ceramics. Figure 6 shows the discharge curves of the PLSZST ceramics with different titanium contents. The discharge current is plotted as a function of time in Fig. 6a. All the samples were charged to 6 kV/mm, followed by

discharge across a load resistance of 3 MΩ. The different discharge times are attributed to the different capacitances of the samples. It is obvious that the sample with titanium content of 13 mol% showed the largest discharge current. Figure 6b and c show the released energy density (J_{re}) and power density (Pd) as a function of discharge time, respectively. The released energy density and power density were calculated according to the following equations:

$$J_{re} = \frac{R}{V}\int I^2(t)\mathrm{d}t, \tag{8}$$

$$Pd = \frac{R}{V}\int \frac{I^2(t)}{t}\mathrm{d}t, \tag{9}$$

where $I(t)$ is the discharge current, t is the discharge time, R is the load resistance, and V is the volume of the sample. From the dependence of the released energy density on the titanium content, it can be seen that the released energy densities increase with increasing titanium content, which is consistent with the hysteresis loop measurements. Moreover, the power densities calculated from the discharged current curves, as shown in Fig. 6c, demonstrate that all the samples can reach almost 300 W/cm^3. It was also concluded that the sample with titanium content of 13 mol% has the largest power density.

CONCLUSIONS

$(Pb_{0.92}La_{0.04}Sr_{0.02})((Zr_{0.70}Sn_{0.30})_{1-x}Ti_x)O_3$ $(0.07 \le x \le 0.13)$ ceramics were synthesized by the conventional solid-state reaction method. The dielectric and energy storage properties of these ceramics were investigated as a function of titanium content. In the investigated composition range, an increase in the titanium content leads to an increase of the tolerance factor, indicating decreased stability of the antiferroelectric phase. In addition, increasing the titanium content led to an increase in the maximum dielectric constant and a decrease in the temperature of the dielectric maximum. *P–E* hysteresis loop measurements showed that both the charged and discharged energy densities gradually increased with increasing titanium content. Moreover, the charge–discharge measurements revealed that, with the increase of titanium content, the released energy densities and power densities also increase.

ACKNOWLEDGEMENTS

This work was supported by the International Science & Technology Cooperation Program of China (No. 2012DFR50560).

REFERENCES

1. J.F. Wang, T.Q. Yang, S.C. Chen, and G. Li, *Mater. Res. Bull.* 48, 3847 (2013).
2. K. Yao, *IEEE Trans. Ultrason. Ferroelectr.* 58, 1968 (2011).
3. Q.F. Zhang, T.Q. Yang, Y.Y. Zhang, J.F. Wang, and X. Yao, *Appl. Phys. Lett.* 102, 222904 (2013).
4. L. Shebanov, M. Kusnetsov, and A. Sternberg, *J. Appl. Phys.* 76, 4301 (1994).
5. S.E. Park, K. Markowski, S. Yoshikawa, and L.E. Cross, *J. Am. Ceram. Soc.* 80, 407 (1997).
6. K. Markowski, S.E. Park, S. Yoshikawa, and L.E. Cross, *J. Am. Ceram. Soc.* 79, 3294 (1996).
7. L. Wang, Q. Li, L.H. Xue, and Y.L. Zhang, *J. Phys. Chem. Solids* 68, 2008 (2007).
8. Q. Zhang, X.L. Liu, Y. Zhang, X.Z. Song, J. Zhu, I. Baturin, and J.F. Chen, *Ceram. Int.* 41, 3030 (2015).
9. M.J. Pan, S.E. Park, K.A. Markowski, W.S. Hackenberger, S. Yoshikawa, and L.E. Cross, *Ferroelectrics* 215, 153 (1998).
10. R.D. Shannon, *Acta Cryst.* A32, 751 (1976).
11. S. Švarcová, K. Wiik, J. Tolchard, H.J.M. Bouwmeester, and T. Grande, *Solid State Ion.* 178, 1787 (2008).
12. X.H. Hao and J.W. Zhai, *J. Phys. D* 40, 7447 (2007).
13. I. Burn and D.M. Smyth, *J. Mater. Sci.* 7, 339 (1972).